Journal of Engineering Research and Reports

Volume 26, Issue 12, Page 231-248, 2024; Article no.JERR.128161
ISSN: 2582-2926

Fault Resistance and Adaptive Analysis of Induction Motors under Voltage Variations in Industrial Applications

Ojimba, Chukwudi Josiah [a], Okpo, Ekom Enefiok [a*] and Attah, Imoh Christopher [b]

[a] Department of Electrical and Electronic Engineering, Akwa Ibom State University, Ikot Akpaden, Nigeria.
[b] Department of Civil Engineering, Akwa Ibom State University, Ikot Akpaden, Nigeria.

Authors' contributions

This work was carried out in collaboration among all authors. All authors read and approved the final manuscript.

Article Information

DOI: https://doi.org/10.9734/jerr/2024/v26i121354

Open Peer Review History:
This journal follows the Advanced Open Peer Review policy. Identity of the Reviewers, Editor(s) and additional Reviewers, peer review comments, different versions of the manuscript, comments of the editors, etc are available here: https://www.sdiarticle5.com/review-history/128161

Original Research Article

Received: 07/10/2024
Accepted: 10/12/2024
Published: 14/12/2024

ABSTRACT

The resilience of three-phase induction motors under fault conditions is critical for the stability and reliability of power systems, especially in industrial and commercial settings where voltage disturbances are common. Induction motors are highly susceptible to under-voltage faults caused by grid instability, load imbalances, or transient faults, which can lead to severe operational issues, reduced motor life, and potential system failures if not properly managed. Understanding how induction motors respond to varying levels of under-voltage disturbances provides essential insights

**Corresponding author: Email: ekomokpo@aksu.edu.ng;*

Cite as: *Chukwudi Josiah, Ojimba, Okpo, Ekom Enefiok, and Attah, Imoh Christopher. 2024. "Fault Resistance and Adaptive Analysis of Induction Motors under Voltage Variations in Industrial Applications". Journal of Engineering Research and Reports 26 (12):231-48. https://doi.org/10.9734/jerr/2024/v26i121354.*

into their adaptive limits and helps identify the thresholds at which protective measures become necessary. This research underscores the importance of integrating advanced fault tolerance designs and adaptive mechanisms to improve system reliability in voltage-sensitive industrial applications. The specification of induction motor used in this analysis are, 7.5Kw rated power, line voltage of 400 volts, and rated speed of 1440 RPM. MATLAB/Simulink simulations software were utilized for this analytical investigation, induction motors were subjected to controlled under-voltage variations applied to single-phase and three-phase systems. The study specifically analyzed the rotor speed, electromagnetic torque, and stator current to evaluate how the motors adapted to faults and how these parameters behaved during fault recovery. Faults were simulated with voltage reductions of 20, 40, and 60%, examining both motor resilience and system recovery upon fault clearance. The findings revealed that at moderate under-voltage levels (20% and 40%), the induction motors adapted effectively by increasing current to maintain adequate performance, with system parameters returning to normal post-fault. However, under extreme 60% under-voltage conditions, the motors experienced significant current surges, causing thermal stress and a failure to return to nominal operating conditions after fault clearance, highlighting the motor's adaptive limit under severe fault scenarios. Additionally, Ohm's law analysis demonstrated how voltage drops and compensatory current increases temporarily reduced effective resistance, facilitating fault resilience under moderate conditions was also analyzed. The study shows that, as the voltage reduce, current increase which cause the resistance to reduce. This study provides insight into the adaptive limits of induction motors in power systems, offering guidelines for implementing effective protection mechanisms in power networks prone to voltage instabilities. The results support improved fault management strategies and motor protection in industrial applications, particularly under varying fault conditions.

Keywords: Induction motor; under-voltage; fault; rotor speed; electromagnetic torque; stator current; simulation; MATLAB/Simulink.

1. INTRODUCTION

Asynchronous motors (Induction Motor) are the most commonly used electrical machines in the industries because of the ruggedness, low maintenance cost, and operating cost with easily available power supply system (Ejiofor et al., 2019). In so many large industries their auxiliary systems such as fans, pumps, conveyor belts, gear boxes are all driven by asynchronous motors (induction motors) which require operation under variable environmental condition (de Almeida et al., 2016; Okpo et al., 2020). To ascertain the performance analysis of the asynchronous motors so many things are to be put in check.

The capacity of the motor as regards to the manufacturer rated value of operation, (parameters) or the rated performance expectancy of the motor by the manufacturer. The parameters can be seen on the name plate of the motor. Despite the ruggedness of the induction motor the operating environment still subject it to stress. There are so many environmental degrading factors such as dust, temperature variations, humidity, continuous operation and heavy loads that effect the motor performance and are capable to create internal faults (Xiao et al., 2018; Sunday et al., 2024).

Induction motor is subject to the supply system. Over voltage and under voltage still play significant and negative effect in the operation of induction motor (Lee, 1999). Environmental stress, heavy duty cycles, load conditions, installation, manufacturer imperfections can reduce the efficiency, also cause malfunction of the induction motor. These lead to high maintenance or repair cost, financial loss and great down time because of breakdown. If these are not checked the operation and maintenance cost will enlarge, bringing revenue loss (Lee, 1999). To analyze the performance of induction motor, fault monitoring, identification, diagnosis and control must be put in place (Okpo et al., 2023; Ezeonye et al., 2022). There are so many factors that bring about faults in an induction motor, overload, ground fault, line to line fault, in balance voltage, over voltage, under voltage, single phasing, and turn to turn short circuit. When one phase of three phase is open this can lead to phasing fault. This gives increase in positive and negative sequence currents and excessive heating. Unbalance supply voltage leads to increase in positive and current components. Ground and line faults are much in

motors more than other power system devices. Turn to turn short circuit and coil open faults can cause current unbalance, other faults broken rotor bar and bearing fault. The faults in Induction motor are group into two, stator faults and rotor faults. Stator winding related faults, are about 37% of the total failures in asynchronous motor.

In most cases, they faults comes as failure in the insulation resistance of the winding. This starts as a turn-to-turn fault, which grow to coil to coil, phase to phase, phase to ground failure and finally cause motor breakdown (Nandi et al., 2005; Okpo et al., 2019; Williams et al., 2023). The factors that cause stator winding fault are, high stator core or winding temperature, loose bracing for end windings, contamination of oil and moisture, short circuit, starting stress, electrical discharge and failure of cooling system (Cruz and Cardoso, 2001). Stator Core are insulated laminated steel in view of minimizing eddy current losses. The stator core lamination is stacked and compressed to avoid vibrations and thermal conductance. Stator core faults are as result of heating of core end region, core melting, lamination vibration for poor core clamping, loosing of core tightening at core end, insulation failure of core, rubbing of rotor and stator during assembly. According to the study of (Cruz and Cardoso, 2001), turns short circuit in induction motor rotor winding cause operational problem such as vibration. The resistance in the opposite poles is identical and heat produce is distributed symmetrically about the rotor forging. When the insulator is damaged due to power failure (Nkan et al., 2023; Nkan and Okpo, 2016), the rotor becomes short circuited and the resistance of the damage coil diminishes. The effect of this large current brings thermal stress to the rotor at minimal cooling and maximum mechanical forces that stresses the rotor bar. Thereafter, the cracked bar will increase in resistance and will over heat the crack, the bar will break completely and arcing will occur. Thus, this will lead to the complete damage of the rotor (Nandi et al., 2005; Siddique et al., 2004). As reported in EPRI (1982) bearing account for 42 - 50% of failure of all motor failures. The cost of bearing in a motor is just about 3% - 10% of the motor total cost but the hidden cost is the downtime. Bearing wears out, and make noise because almost all the stresses of motor rest on it through the shaft.

Faulty bearing cause over heating of the motor and vibration. Rolling bearings are considered to be the main component of rotating machinery. However, bearings are used in several mechanical and electrical applications, including induction motors, turbines, medical devices, cars and trucks, engines, automobile industry, and aerospace. Importantly, any failure of this basic component can lead to a serious breakdown of rotating machines. Rolling bearing faults could be categorized by two main factors, location of the fault and nature of the fault. For location category, five main faults occurred including, imbalance shaft faults, ball faults, inner race faults, outer race faults, and cage faults. For nature category, two main faults are considered, including cyclic faults and noncyclic faults. Condition monitoring and Fault detective diagnose of bearing element bearings of rotating machines are widely used to follow up the operation condition of the machine. However, the main task of condition monitoring and Fault detection diagnose is to diagnose faults and failures (Cruz and Cardoso, 2001; Udoh et al., 2024).

As a result, any failure may cause a serious breakdown, which increases the maintenance cost and leads to heavy losses. Recently, various methodologies of condition monitoring and Fault detective diagnose of Induction motor have been discussed. Moreover, several data and model-based techniques have been introduced including signal processing-based techniques, image processing-based techniques, intelligent techniques, data fusion techniques, data mining techniques, and expert system techniques. All those techniques have used specific analyses to develop the Fault detection diagnose methodology to arrive at efficient and accurate results. As the analyses used in those studies include chemical analysis, electrical analysis, and mechanical analysis, in more details, temperature analysis, vibration analysis, noise analysis, radio-frequency (RF) analysis, infrared analysis, current and voltage analysis, electromagnetic field analysis, oil analysis pressure analysis, ultrasound analysis, and sound and acoustic emission analysis.

However, most electrical and mechanical signals are nonlinear and nonstationary signal. Eccentricity is the air gap that exists between the rotor and stator. A certain eccentricity must be maintained in a rotating machine. Normally induction motor eccentricity is smaller than other types of motors or machines. This make induction motor more sensible than other motors

when there is change in the length of the air gap. There should be comprehensive and continuous monitoring of running induction motors. A continuous condition monitoring scheme shall provide adequate warning of serious failure of its critical components. The parameters monitored in induction motor are voltage, current, rotor speed by this one can predict and identify, stator ground failure, inter turn fault, stall, overload, bearing failure, rotor defects and shaft eccentricity (Diji et al., 2013a; Ekpo, 2012). While induction motor is running, its parameters may change with influences of inner wear and outer conditions. The changes of the motor temperature rise can affect the rotor resistance value, it may increase by 50%. With the temperature rise, the rotor inductance will also change value because of magnetic saturation. Due to effective monitoring, faults can be identified and diagnose (Etim et al., 2024; Diji et al., 2013b).

The most important characteristic of any condition monitoring scheme is its quickness of detection. Different types of faults usually progress from incipient to a very advanced stage in a different manner. For the detection of early rotor failure, only partially broken rotor bars are taken into account, whereas fully broken rotor bars are considered a developed fault. This is because once a bar is completely fractured, the failure spreads rapidly to adjacent bars and subsequently damages the stator winding causing irreparable damage. In the case of bearing faults, the early fault condition is considered when the diameter of the fracture in the inner or the outer race is less than 12.5% of the diameter of the bearing ball, since from then on, the bearing stroke undergoes great alterations and alters the rotor symmetry, making the failure to be considered as developed or advanced. The stator failure is considered in an early condition before exceeding 3.33% of the turns in the stator phase. Once the short circuit begins, it propagates rapidly in a very short time. Unless detected early enough, it might lead to catastrophic consequences. Faults detected at advanced stages are far more likely to cause unplanned breakdowns in the line production than those detected while the failure is still at an early stage (Li et al., 2000; Bassey et al., 2024).

Techniques that can detect faults at an early stage are very desirable for the possibility of correcting the faulty condition entirely with low impact to the production line. For early detection to be an effective and practical approach, techniques must satisfy three basic requirements. First, the detection analysis should be able to distinguish faulty IM from healthy IM cases with a high degree of accuracy. Second, the detection should be possible before the fault progresses to a developed stage, when the propagation is accelerated, and preventive actions are less effective. There are many methods of identification or detection of fault, Artificial Neural network, fast Fourier transforms, motor current signature analysis, Wavelet and Complex Park vectors (Abhinandan and Sidram, 2017). These methods are based on spectral analysis of stator current.

In this work, a 7.5kw, 400 volts and 1440 RPM three phase induction motor were used to identify the possible faults and induction motor adaptation to these faults. MATLAB and Simulink software were utilized for this analytical investigation.

2. METHODOLOGY

From the flow chart above, we start by reviewing existing research on the performance of three-phase induction motors, specifically focusing on resistance and fault adaptation. This helps us understand what has already been done, key challenges, and how faults affect motor performance, this sets the theoretical foundation for the work. After the literature review, we determine the appropriate capacity of the three-phase induction motor for the simulations, this involves selecting the right motor specifications (power rating, torque, resistance, etc.) that best match the simulation needs, ensuring realistic results. Appropriate software tools for modeling, simulating, and analyzing of the system was review and MATLAB/Simulink simulation soft was chosen because it provides a comprehensive environment for modeling, simulating, and analyzing complex systems. It's also allowed for detailed modeling of the behavior of induction motors under different operating conditions as well as integrating seamlessly with other MATLAB toolboxes and software packages, enabling engineers to perform multidomain simulations and incorporate additional functionalities such as signal processing, control system design, and optimization. After chosen the software, the necessary parameters (such as motor resistance, stator and rotor inductances, load conditions, fault conditions) were enter with the help of function blocks to model the three-phase

induction motor and surrounding system as shown in Fig. 1. With the built model, the simulation was run to analyze the motor's behavior under various conditions. Our focus in particular was how the motor responds to faults, examining how the resistance changes and affects the motor's ability to resist and adapt to the fault. After simulation, we perform a comparative analysis by studying how different levels of motor resistance impact the motor's performance during faults, compare the results with motors of varying resistance levels and other performance criteria to assess fault adaptation and resilience using graph.

3. ANALYTICAL MODELLING OF SCIM

A squirrel cage induction motor (SCIM) is an AC machine whose operating speed under load conditions is always slightly less than its synchronous speed. It functions based on the principle of electromagnetic induction. The steady-state performance of SCIM has been extensively analyzed in prior studies (Gonzalez and Arjona, 2014), while other works (Ejiofor et al., 2019; Jha et al., 2016), have outlined design strategies to achieve the desired operational performance.

The voltage equations of SCIM, expressed in the dq0 reference frame using the analytical method, are provided in equations (1)-(4):

$$v_{ds} = R_s i_{ds} \frac{d\lambda_{ds}}{dt} - \omega_e \lambda_{qs} \quad (1)$$

$$v_{qs} = R_s i_{qs} \frac{d\lambda_{qs}}{dt} - \omega_e \lambda_{ds} \quad (2)$$

$$v_{dr} = 0 = R_r i_{dr} \frac{d\lambda_{dr}}{dt} - (\omega_e - \omega_r)\lambda_{qr} \quad (3)$$

$$v_{qr} = 0 = R_r i_{qr} \frac{d\lambda_{qr}}{dt} - (\omega_e - \omega_r)\lambda_{dr} \quad (4)$$

where d is the direct axis, q is the quadrature axis, $v_{ds}$is the d-axis stator voltage, v_{qs} is the q – axis stator voltage, v_{dr} is d – axis rotor voltage, v_{qr} is q-axis rotor voltage, i_{ds} is the d-axis stator current, i_{qs} is the q-axis stator current, i_{dr} is d-axis rotor current, i_{qr} is q-axis rotor current, R_s is the stator resistance, R_r is the rotor resistance, ω_e is the angular velocity of the reference frame, ω_r is the angular velocity of the rotor, and λ_{qs}, λ_{ds}, λ_{qr}, and λ_{dr} are flux linkages. It is assumed that the induction motor analyzed is a squirrel cage machine, leading to the rotor voltage in (3) and (4) being zero. The flux linkages in (1-4) can be written as:

$$\lambda_{ds} = L_s i_{ds} + L_m i_{dr} \quad (5)$$

$$\lambda_{qs} = L_s i_{qs} + L_m i_{qr} \quad (6)$$

$$\lambda_{dr} = L_r i_{dr} + L_m i_{ds} \quad (7)$$

and

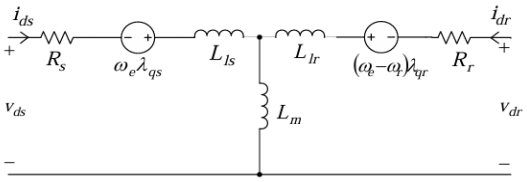

d-axis equivalent circuit

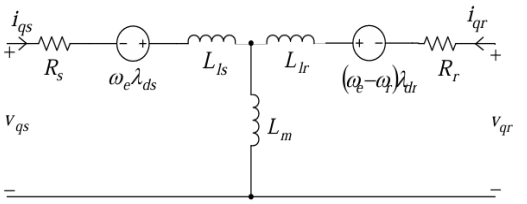

q-axis equivalent circuit

Picture 1. d-q equivalent circuit of the induction motor (Batool and Ahmad, 2013)

$$\lambda_{qr} = L_r i_{qr} + L_m i_{qs} \quad (8)$$

Where L_r is the rotor self-inductance, L_s is the stator self-inductance, L_m is the magnetizing inductance, L_{Ir} is the rotor leakage inductance, and L_{Is} is the stator leakage inductance. The self-inductances in (5-8) can be expressed as:

$$L_s = L_m + L_{Is} \quad (9)$$

and

$$L_r = L_m + L_{Ir} \quad (10)$$

The currents equations can be written as:

$$i_{ds} = \frac{\lambda_{ds} - L_m i_{qr}}{L_s} \quad (11)$$

$$i_{qs} = \frac{\lambda_{qs} - L_m i_{qr}}{L_s} \quad (12)$$

$$i_{dr} = \frac{\lambda_{dr} - L_m i_{ds}}{L_r} \quad (13)$$

and

$$i_{qr} = \frac{\lambda_{qr} - L_m i_{qs}}{L_r} \quad (14)$$

After making substitutions, the currents can be expressed in terms of flux linkages as:

$$i_{ds} = \frac{L_r}{L_r L_s - L_m^2}\lambda_{ds} - \frac{L_m}{L_r L_s - L_m^2}\lambda_{dr} \quad (15)$$

$$i_{qs} = \frac{L_r}{L_r L_s - L_m^2}\lambda_{qs} - \frac{L_m}{L_r L_s - L_m^2}\lambda_{qr} \quad (16)$$

$$i_{dr} = \frac{L_s}{L_r L_s - L_m^2}\lambda_{dr} - \frac{L_m}{L_r L_s - L_m^2}\lambda_{ds} \quad (17)$$

and

$$i_{qr} = \frac{L_s}{L_r L_s - L_m^2}\lambda_{ds} - \frac{L_m}{L_r L_s - L_m^2}\lambda_{qs} \quad (18)$$

Three-phase voltages can be converted to the two-phase stationary frame using the following relationship:

$$\begin{bmatrix} v_{qs}^s \\ v_{ds}^s \end{bmatrix} = \begin{bmatrix} 1 & 0 & 0 \\ 0 & \frac{-1}{\sqrt{3}} & \frac{1}{\sqrt{3}} \end{bmatrix} \begin{bmatrix} v_{an} \\ v_{bn} \\ v_{cn} \end{bmatrix} \quad (19)$$

where the superscript s in (19) refers to the stationary frame. The voltages can be converted from the two-phase stationary frame to the synchronously rotating frame using the following:

$$v_{qs} = v_{qs}^s cos\theta_e - v_{ds}^s sin\theta_e \quad (20)$$

and

$$v_{ds} = v_{qs}^s sin\theta_e + v_{ds}^s cos\theta_e \quad (21)$$

The current variables are given as:

$$i_{qs}^s = i_{qs} cos\theta_e + i_{ds}^s sin\theta_e \quad (22)$$

$$i_{ds}^s = i_{qs} sin\theta_e + i_{ds}^s cos\theta_e \quad (23)$$

The current equation will now become:

$$\begin{bmatrix} i_a \\ i_b \\ i_c \end{bmatrix} = \begin{bmatrix} 1 & 0 \\ \frac{-1}{2} & \frac{-\sqrt{3}}{2} \\ \frac{-1}{2} & \frac{\sqrt{3}}{2} \end{bmatrix} \begin{bmatrix} i_{qs}^s \\ i_{ds}^s \end{bmatrix} \quad (24)$$

The electromagnetic torque equation is given by:

$$T_e = \frac{3}{2}\frac{p}{2} L_m (i_{ds} i_{dr} - i_{ds} i_{qr}) \quad (25)$$

Where P is the number of poles and T_e is the electromagnetic torque. And the mechanical system equation is given by:

$$\frac{d}{dt}\omega_m = \frac{1}{j}(T_e - T_l - B_{\omega m}) \quad (26)$$

Where;

$$\omega_r = \frac{p}{2}\omega m$$

$$\frac{d}{dt}\omega_r = \frac{p}{2j}(T_e - T_l - B_{\omega r}) \quad (27)$$

From Table 1, the relationship between load torque (T_l) or shaft torque T_{sh} in Nm, power output (p_{output}) in (W) and angular velocity (ω) in rad/secs is given by;

$$T_l \; or \; T_{sh} = \frac{p_{output}}{\omega} \quad (28)$$

The expression for motor power is derived by the following relationship

$$p_{output} = T_s * \omega \quad (29)$$

Where the motor output power is given as 37000w, and angular velocity is defined by the following expression

$$(\omega) = \frac{2*\pi*N}{60} \quad (30)$$

Where the value of π in radians is given as 3.142 and speed of the asynchronous motor is rated at 1440RPM.

The angular velocity can be calculated as follows

Angular velocity $(\omega) = \frac{2*\pi*N}{60}$

∴ Angular $(\omega) = \frac{2*3.142*1440}{60} = 151\; rad/secs$

Slip = $\frac{\omega_s - \omega}{\omega_s}$ $where\; \omega_s = 2*\pi*50$

Slip = $\frac{314-151}{314} = 0.52$

Given the motor output power to be 7500w and ω = 151rad/secs, the full load torque can be calculated as follows;

$$T_l = \frac{7500}{151} = 49.7\; N-m$$

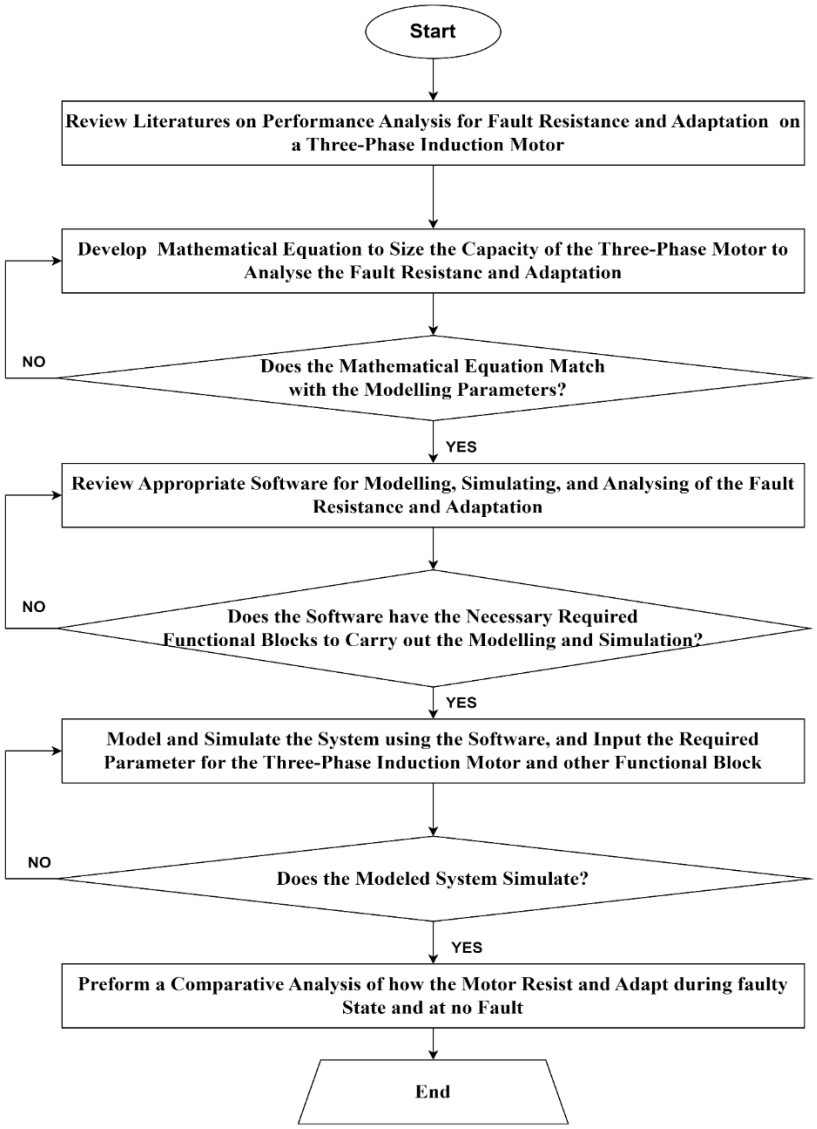

Fig. 1. Flow chart of the research work

Table 1. Specification of the asynchronous machine rated parameters

Number	Parameters	Value
1	Input power of the motor	7.5Kw
2	Motor input voltage	400V
3	Frequency	50Hz
4	Motor speed	1440 RPM
5	Mechanical power	7.5Kw
6	Stator resistance	0.7384Ω
7	Stator inductance	0.003045 mH
8	Rotor resistance	0.7402Ω
9	Rotor inductance	0.003045 mH
10	Mutual inductance	0.1241H
11	Inertia(J)	0.0343 (kg.m^2)
12	Friction factor(F)	0.000503 $(N.m.s)$
13	Number of pole pair	4
14	Initial condition	10000000

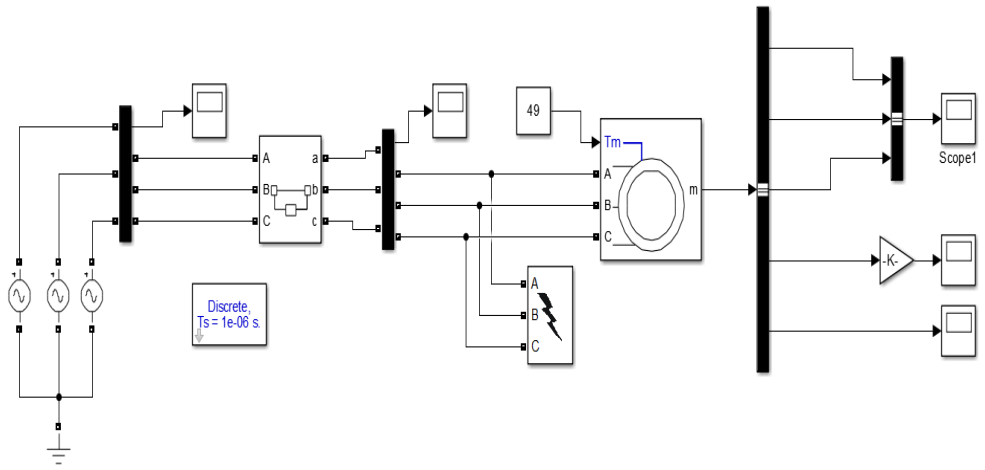

Fig. 2. SIMULINK model of asynchronous motor for fault resistance and adaptation analysis

The calculated angular velocity of ω = 151 rad/s = 151, affects the motor's torque output and slip. At this speed, the slip is 1%, which is consistent with typical operating conditions for this induction motor. This speed is also used in the torque-speed characteristic block of the Simulink model to determine the motor's steady-state performance under a specific load condition."

The modeled was simulated and their output waveform was studied and improve upon where it is necessary. the Simulink model of asynchronous motor for fault resistance and adaptation analysis is shown in Fig. 2.

4. RESULTS AND DISCUSSION

In this chapter, the results of the simulations are presented, focusing on the impact of various under voltage variations on the performance of the three-phase induction motor under fault conditions. The primary aim of this analysis is to assess the motor's adaptive behavior and resistance to faults by observing key performance indicators, including current, speed, electromagnetic torque, and resistance variations.

To investigate the motor's adaptability to faults, a series of under voltage variations was introduced systematically. Each variation aimed to emulate real-world fluctuations and stress the motor under increasingly adverse conditions. The results provide insight into the motor's dynamic response, resilience, and recovery patterns when subjected to these electrical stresses. The voltage variations are shown in Table 2.

From Table 2, recall that when dealing with a three-phase voltage supply to a start connected induction motor, the given voltage is in rms which typically refers to the line-to-line voltage. To find the maximum voltage V_{max} for the star-connected system, we need to determine the phase voltage first. The relationship between line-to-line voltage V_{LL} and line-to-neutral (phase) voltage V_{LN} in a three-phase system is given by:

$$V_{LN} = \frac{V_{LL}}{\sqrt{3}} \tag{31}$$

Table 2. Under-voltage percentage variations

S/N	% Variations	Voltage drops (V)	New voltage value (V)
1	10	0.1 * 325 = 33	325 – 33 = 292
2	20	0.2 * 325 = 65	325 – 65 = 260
3	30	0.3 * 325 = 98	325 – 98 = 227
4	40	0.4 * 325 = 130	325 – 130 = 195
5	50	0.5 * 325 = 163	325 – 163 = 162
6	60	0.6 * 325 = 195	325 – 195 = 130
7	70	0.7 * 325 = 228	325 – 228 = 97
8	80	0.8 * 325 = 260	325 – 260 = 65
9	90	0.9 * 325 = 293	325 – 293 = 32
10	100	1.0 * 325 = 325	325 – 325 = 0

Given that $V_{LL} = 400V$

$$V_{LN} = \frac{400}{\sqrt{3}} = 230\ V$$

Now, we can calculate the peak voltage V_{max} from the phase voltage V_{LN}

$$V_{max} = V_{LN} * \sqrt{2}$$

So,

$$V_{max} = 230 * \sqrt{2}$$

$$V_{max} = 230 * 1.414$$

$$V_{max} = 325V$$

Therefore, the maximum voltage V_{max} for a star-connected three-phase induction motor with a 400 V three-phase supply is approximately 325 volts. The analysis will cover no under-voltage variation (normal condition), 20% under-voltage variation, 40% under-voltage variation, and 60% under-voltage variation. Single line-to-ground fault (SLG) and three line-to-ground faults (LLLG) will be analyzed as well.

4.1 Normal Operating Condition (Without Under-Voltage Variation)

Under normal voltage conditions, the induction motor operates at its designed input power level, leading to stable performance in rotor speed, electromagnetic torque, and stator current. Figs 3a, 3b, and 3c present the simulation result with normal operating condition

As seen in Fig. 3a, at normal voltage, the rotor speed remains close to synchronous speed, with only a slight slip inherent in induction motor operation. This small deviation from synchronous speed is necessary to induce torque. The stability in rotor speed under normal conditions reflects the motor's efficient operation without needing to compensate for voltage fluctuations.

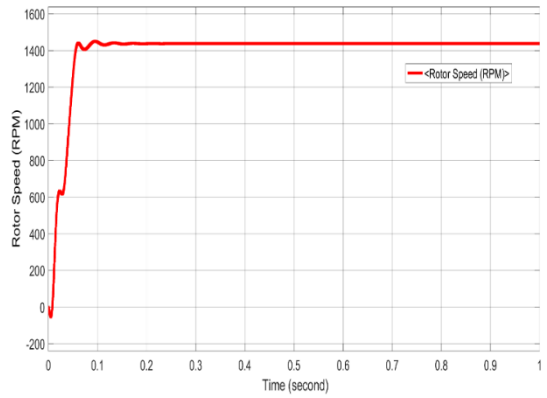

(a)

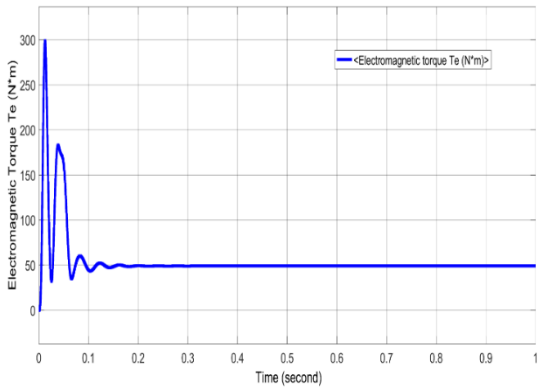

(b)

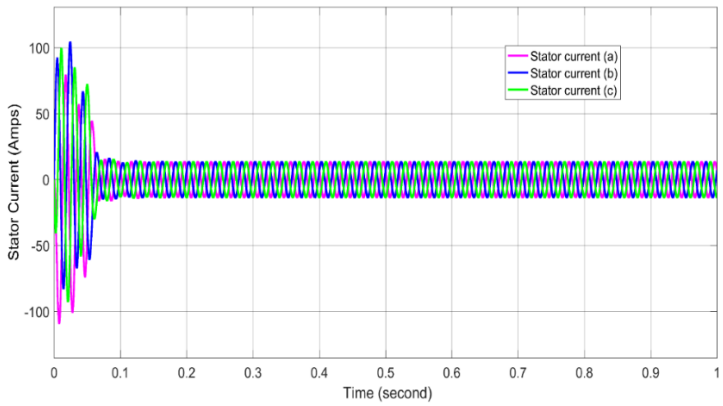

(c)

Fig. 3. (a) Rotor speed simulation result at normal operating condition. (b) Electromagnetic torque simulation result at normal operating condition. (c) Stator currents simulation result at normal operating condition

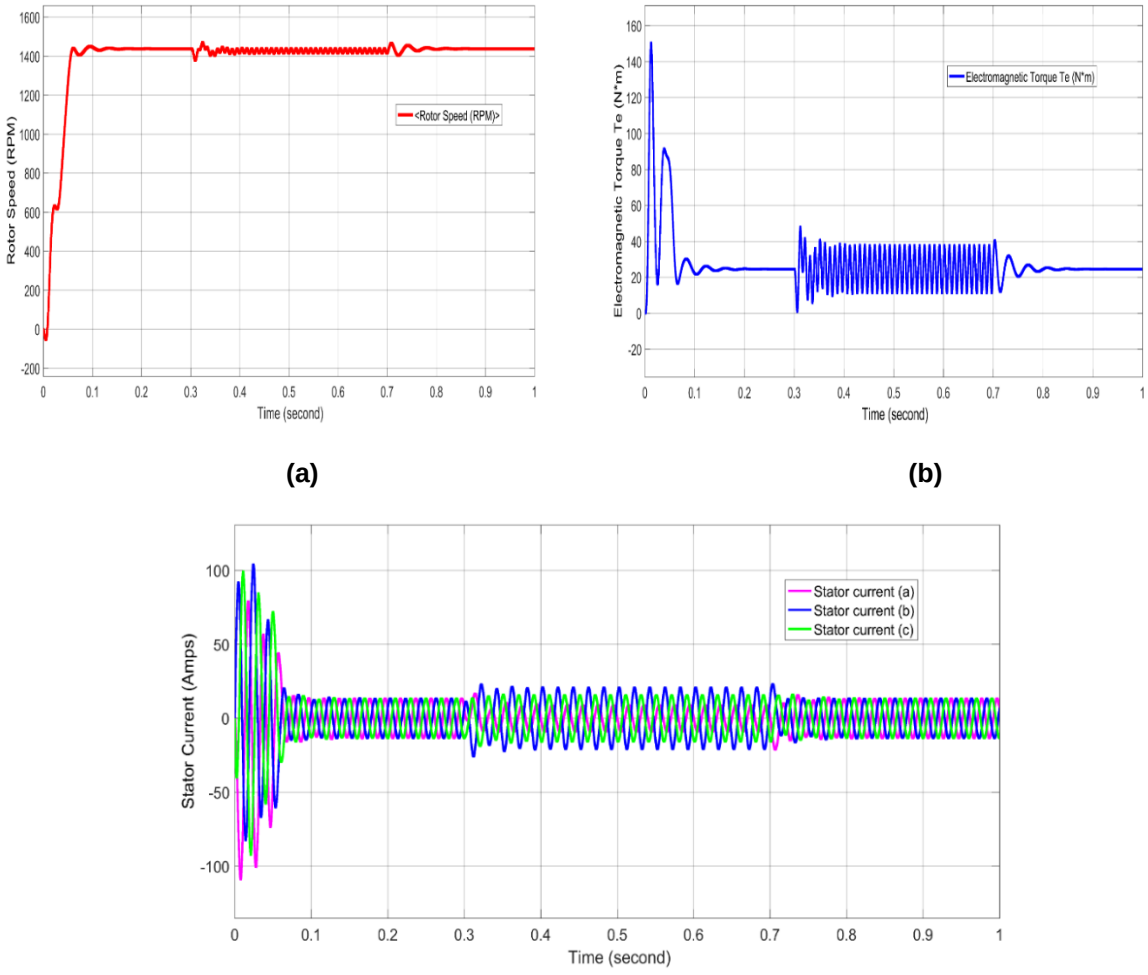

Fig. 4. (a) Rotor speed simulation result at 20% under-voltage variation (LG). (b) Electromagnetic torque simulation result at 20% under-voltage variation (LG). (c) Stator currents simulation result at 20% under-voltage variation (LG)

As seen in Fig. 3b, in a steady-state condition without any voltage disturbance, the electromagnetic torque is stable and matches the load requirements. This stable torque indicates that the motor's power conversion is optimal, with minimal oscillations in torque, which would otherwise indicate the need to adjust for voltage changes.

It can be seen in Fig. 3c, that the stator current also maintain a balanced and consistent voltage supply, the stator current remains stable at its rated value. This indicates minimal electrical stress on the motor, as it draws only the necessary current to sustain operation. The current waveform remains smooth and free of the surges or oscillations that typically occur during voltage fluctuations.

4.2 Simulated Condition: 20% Under-Voltage Variation on Single Phase to Ground

This voltage drop introduces an unbalanced condition, impacting the motor's performance and causing asymmetric magnetic flux in the stator, which in turn affects rotor speed, electromagnetic torque, and stator current. Fig. 4a, 4b, and 4c present the simulation result with 20% under-voltage variation.

As seen in Fig. 4a, with a 20% voltage drop in a single phase, the rotor speed experiences a slight reduction in speed. The unbalanced supply voltage occurs at 0.3 second till 0.7 seconds, this weakens the overall magnetic field strength, causing the motor to lose some synchronism and

slip slightly more than it would under balanced conditions. While the rotor speed decreases, it generally remains within the operational range, but with minor fluctuations due to the unbalanced torque production.

As seen in Fig. 4b, electromagnetic torque becomes uneven and less stable. The single-phase voltage drops results in fluctuating torque because the reduced magnetic field affects one phase differently, causing oscillations in torque production. The fluctuating torque under this condition causes vibrations and potential mechanical stresses within the motor.

It can be seen in Fig. 4c, the stator current increases significantly in the affected phase to compensate for the voltage drop. This uneven current distribution leads to unbalanced heating in the stator windings which increase the risk of insulation stress in the affected phase. The waveform of the stator current shows increased distortion and potential spikes due to the compensatory draw from the weakened phase.

4.3 Simulated Condition: 40% Under-Voltage Variation on Single Phase to Ground

The 40% voltage drop introduces a substantial imbalance, leading to pronounced disruptions in motor stability. This section details how the rotor speed, electromagnetic torque, and stator current resists and adapt to the fault.

As seen in Fig. 5a, the substantial reduction in one phase's voltage weakens the magnetic field strength and disrupts the balance needed for synchronous operation. This disturbance leads to increased slip, causing the rotor to slow down noticeably with speed continuing to fluctuate as the motor attempts to maintain stability.

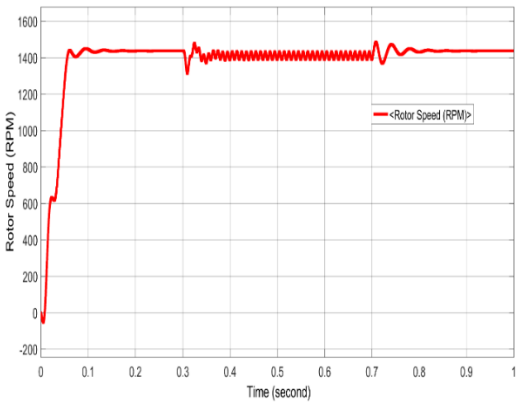

(a)

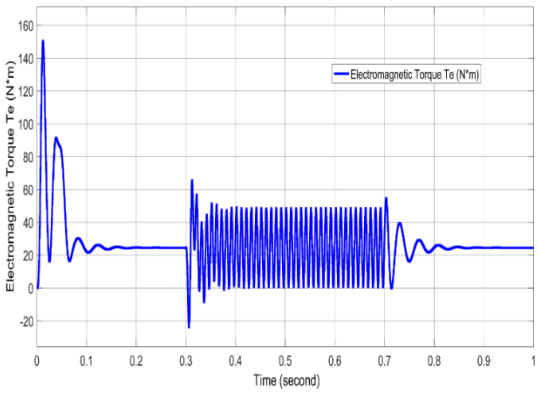

(b)

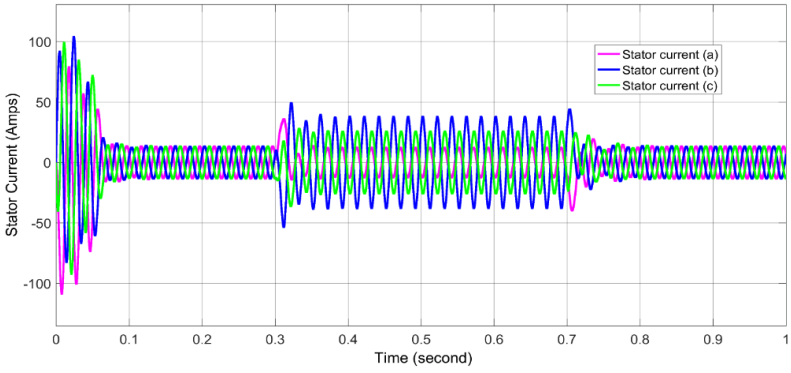

(c)

Fig. 5. (a) Rotor speed simulation result at 40% under-voltage variation (LG). (b) Electromagnetic torque simulation result at 40% under-voltage variation (LG). (c) Stator currents simulation result at 40% under-voltage variation (LG)

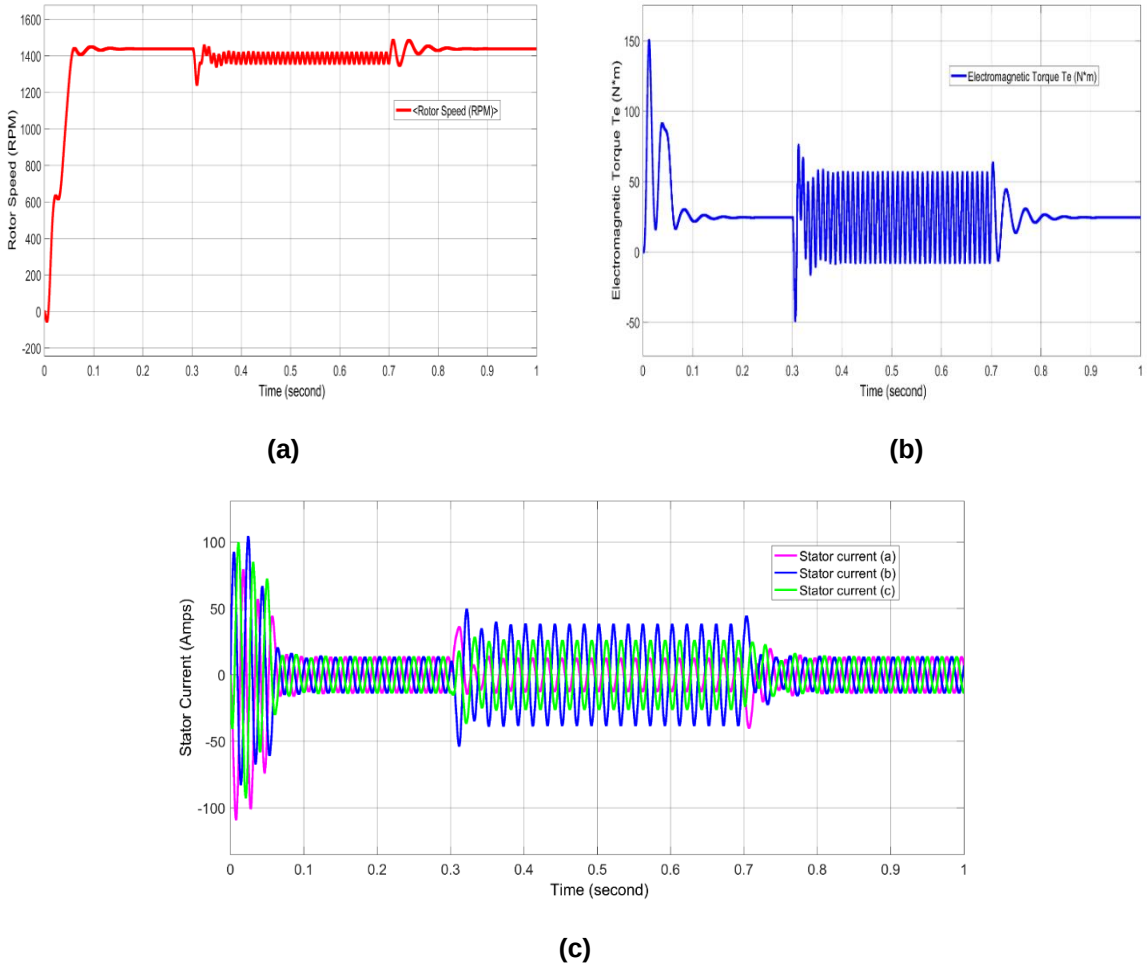

Fig. 6. (a) Rotor speed simulation result at 60% under-voltage variation (LG). (b) Electromagnetic torque simulation result at 60% under-voltage variation (LG). (c) Stator currents simulation result at 60% under-voltage variation (LG)

As seen in Fig. 5b, the electromagnetic torque experiences large, erratic fluctuations due to the asymmetry in magnetic field distribution. This uneven torque production results from the weakened field in the under-voltage phase, causing dips and surges that produce noticeable vibrations and impact the mechanical integrity of the motor.

It can be seen in Fig. 5c, the stator current in the affected phase increases drastically as the motor tries to compensate for the voltage loss. leading to overheating in the affected phase.

4.4 Simulated Condition: 60% Under-Voltage Variation on Single Phase to Ground

This extreme under-voltage scenario creates severe imbalance in the motor's electrical parameters. Fig. 6a, 6b, and 6c present a detailed explanation of the impacts on rotor speed, electromagnetic torque, and stator current.

As seen in Fig. 6a, the rotor speed experiences a pronounced decrease as the magnetic field strength is heavily reduced in the affected phase. With the remaining two phases at normal voltage, the imbalance leads to substantial slip, causing the rotor speed to drop well below its normal operating range.

As seen in Fig. 6b, electromagnetic torque becomes highly unstable, with sharp oscillations as the motor's magnetic field is heavily disrupted leading to severe fluctuation.

It can be seen in Fig. 6c, the stator current in the affected phase increases significantly in an attempt to compensate for the weakened power

input leading to large current spikes and oscillations.

4.5 Simulated Condition: 20% Under-Voltage Variation on Three-Phase to Ground

The 20% reduction across all three phases represents a balanced but reduced voltage condition, affecting motor performance differently than single-phase voltage drops. Fig. 7a, 7b, and 7c present a detailed explanation of the impacts on rotor speed, electromagnetic torque, and stator current.

As seen in Fig. 7a, the rotor speed decreases but remains relatively stable compared to single-phase faults. Since the voltage reduction is balanced, the motor experiences less fluctuation in speed and can maintain a controlled, albeit lower, speed.

As seen in Fig. 7b, electromagnetic torque reduction is more uniform and lacks the severe oscillations seen in single-phase faults, as all three phases contribute equally to torque production.

It can be seen in Fig. 7c, the increase in stator current is relatively smooth and balanced across the phases, lacking the severe phase-specific current spikes typical in single-phase faults.

4.6 Simulated Condition: 40% Under-Voltage Variation on Three-Phase to Ground

The 40% symmetrical voltage drop results in a considerable reduction in motor performance, affecting the induction motor's core parameters. This section outlines the impacts on rotor speed, electromagnetic torque, and stator current.

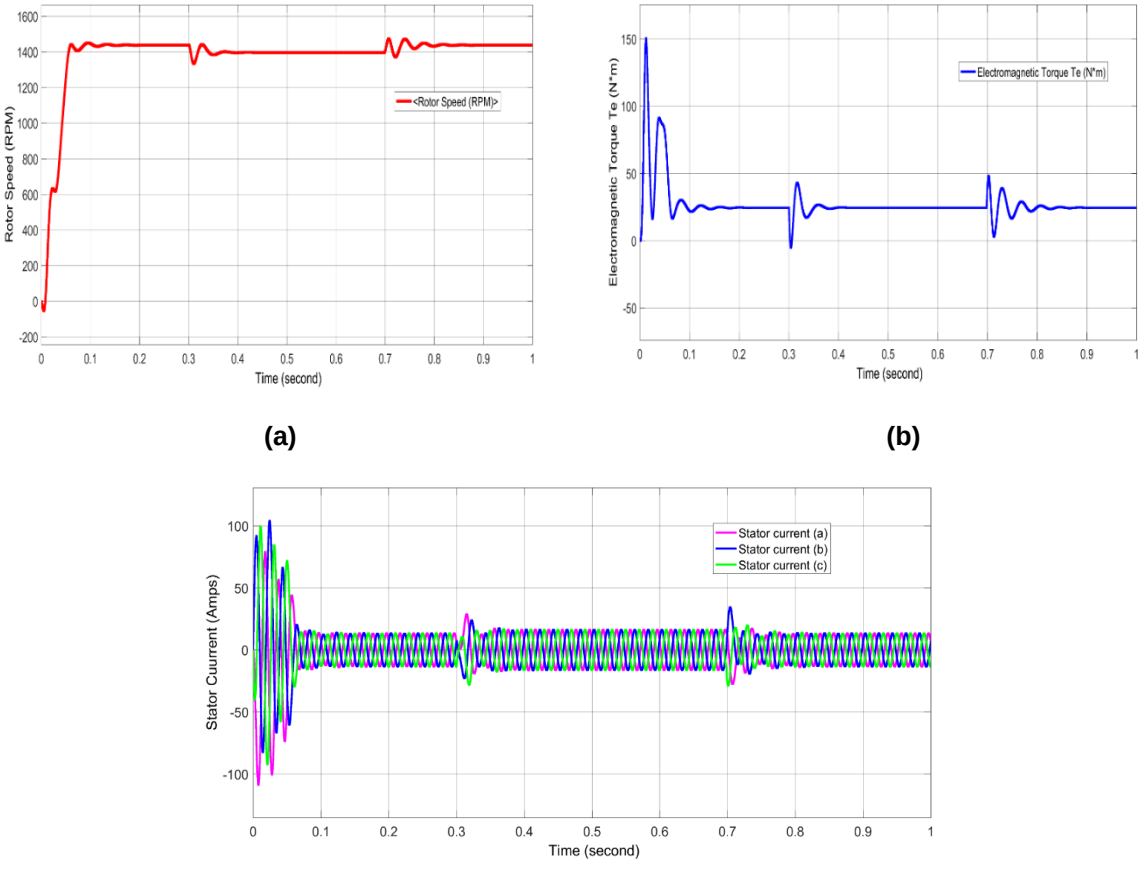

Fig. 7. (a) Rotor speed simulation result at 20% under-voltage variation (LLLG). (b) Electromagnetic torque simulation result at 20% under-voltage variation (LLLG). (c) Stator currents simulation result at 20% under-voltage variation (LLLG)

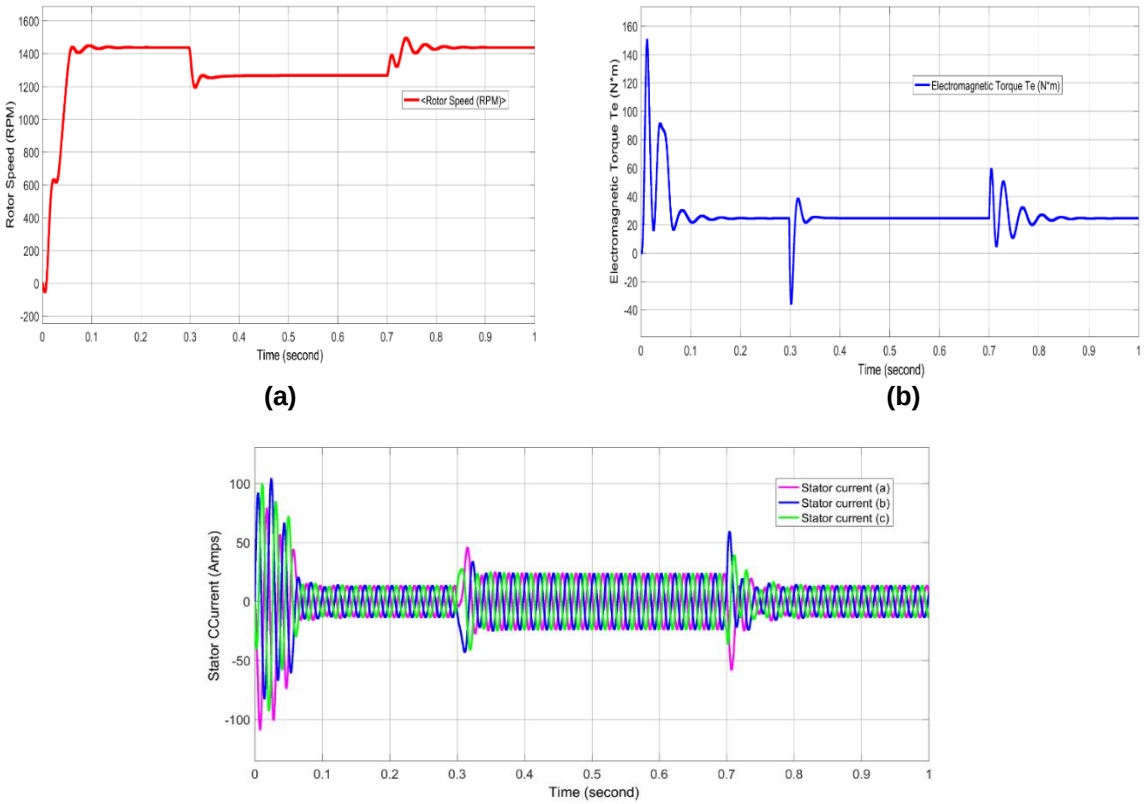

Fig. 8. (a) Rotor speed simulation result at 40% under-voltage variation (LLLG). (b) Electromagnetic torque simulation result at 40% under-voltage variation (LLLG). (c) Stator currents simulation result at 40% under-voltage variation (LLLG)

As seen in Fig. 8a, the balanced yet low voltage supply causes a large increase in slip, leading to reduced rotor speed well below its typical operating range. The motor still run but at a much lower speed, struggling to reach the synchronous speed due to the significant reduction in electromagnetic field strength.

As seen in Fig. 8b, the motor's ability to generate sufficient torque to meet the load demand is severely compromised. The torque reduction accompanied by minor oscillations as the motor tries to adjust, leading to inadequate torque production and potential performance instability.

It can be seen in Fig. 8c, the increase in current is consistent across all three phases, given the symmetrical nature of the fault, but the magnitude of current is much higher than in the 20% under-voltage case.

4.7 Simulated Condition: 60% Under-Voltage Variation on Three-Phase to Ground

The severe 60% symmetrical voltage drop places considerable strain on motor performance. This section details the effects on rotor speed, electromagnetic torque, and stator current during the fault.

As seen in Fig. 9a, due to the significant drop in voltage across all three phases, the rotor speed decreases drastically, as the induction motor cannot maintain its typical operational speed under such low voltage conditions.

As seen in Fig. 9b, the electromagnetic torque suffers a major reduction, as the motor's capability to produce torque is severely impaired by the low input voltage.

It can be seen in Fig. 9c, after the fault was lifted at 0.7 seconds, the system could not return back to its original position given the symmetrical

nature and how serve the fault is, this increase is uniform across all three phases but substantial, with the motor drawing far more current than normal in an attempt to maintain power.

4.8 Fault Adaptation and Resistance of the Induction Motor

In this analysis, we focus on the motor response and adaptation to faults, examining its ability to return to normal operating conditions after each fault is lifted, except in the case of the 60% three-phase under-voltage variation. Here's an analysis based on Ohm's Law, relating voltage, current, and resistance in the context of motor performance. The analysis of the motor behavior in terms of resistance based on Ohm's Law is given by:

$$V = IR$$

where V is the voltage, I is the current, and R is the resistance

At 20% variation (325V to 260V) the resistance can be calculated as follow:

$$V = IR, V = 260V \; and \; I = 30A$$

$$R = \frac{V}{I} = \frac{260}{30} = 8.7\Omega$$

At 40% variation (325V to 195V) the resistance can be calculated as follow:

$$V = IR, V = 195V \; and \; I = 45A$$

$$R = \frac{V}{I} = \frac{195}{45} = 4.3\Omega$$

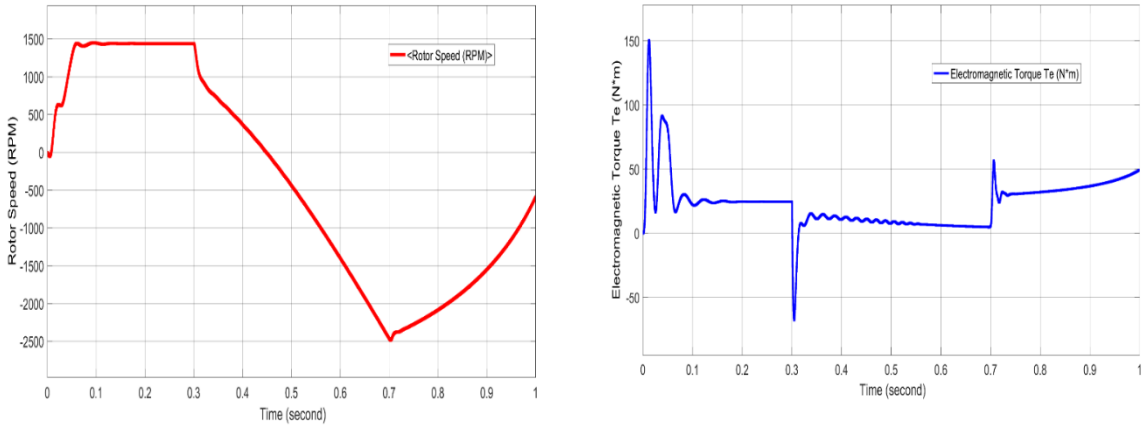

(a) (b)

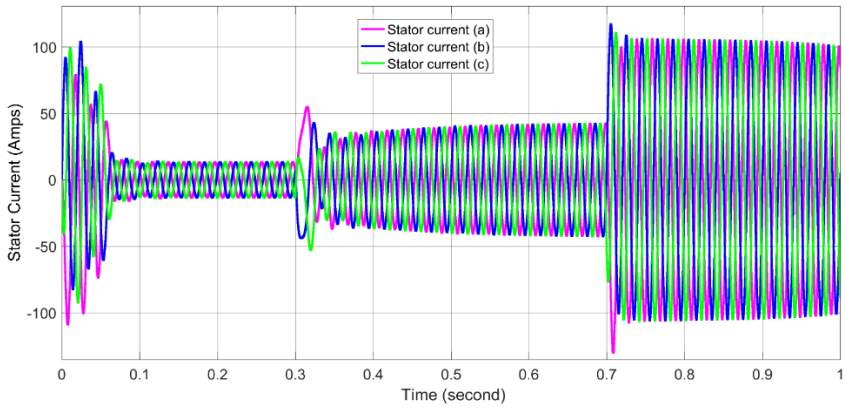

(c)

Fig. 9. (a) Rotor speed simulation result at 60% under-voltage variation (LLLG). (b) Electromagnetic torque simulation result at 60% under-voltage variation (LLLG). (c) Stator currents simulation result at 60% under-voltage variation (LLLG)

Table 3. Fault adaptation and resistance table

S/N	% Variations	Voltage drops (V)	Current (amps)	Resistance (ohms)
1	20	325-260	30	8.7
2	40	325-195	45	4.3
3	60	325-130	70	1.9

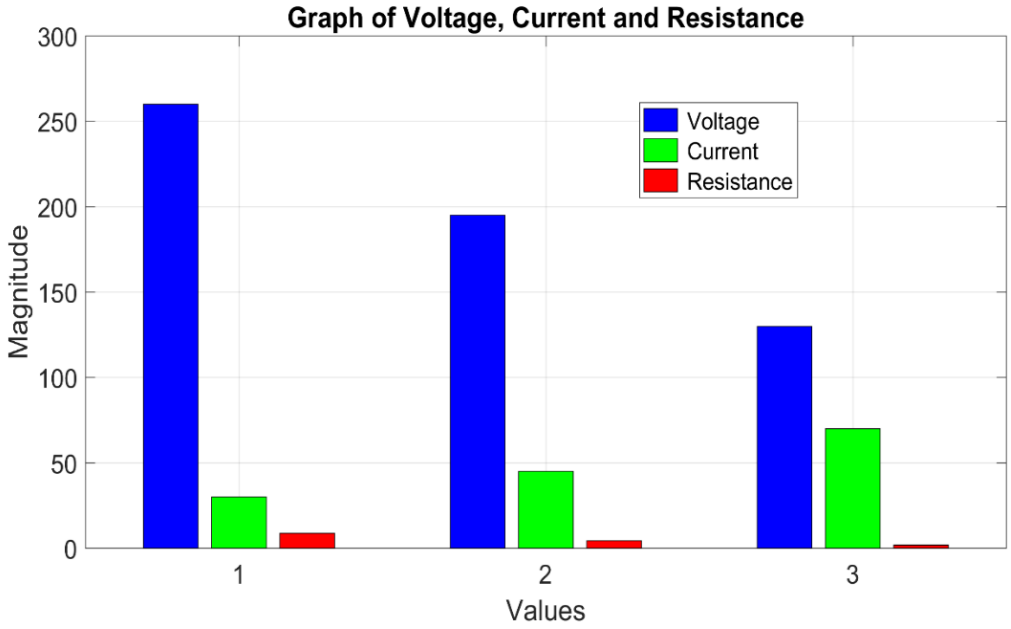

Fig. 10. Graph of Voltage, Current and Resistance

At 60% variation (325V to 130V) the resistance can be calculated as follow:

$$V = IR, V = 130V \; and \; I = 70A$$

$$R = \frac{V}{I} = \frac{130}{70} = 1.9\Omega$$

The relationship between voltage, current, and resistance based on Ohm's law provides a foundational understanding of how the motor adapts to different under-voltage conditions. The adaptive table and graphical representation are presented in Table 3 and Fig. 10 respectively.

As seen in Fig. 10, at 20% voltage variation, the current increase as well while the motor resistivity decrease, at 40% voltage variation, the motor current further increases leading to decrease in motor resistance, at 60% voltage variation, the increase in motor current is more serve leading to drastic decrease in resistance. At the point the motor could not adapt to the faulty condition after the fault was lifted off the motor.

5. CONCLUSIONS

This project demonstrated that three-phase induction motors exhibit varying degrees of resilience to under-voltage faults, with adaptation thresholds influenced by the severity of the voltage drop. Through a series of MATLAB/Simulink simulations, it was shown that at moderate under-voltage levels (20% and 40%), motors effectively adapt by increasing current to compensate for power loss, allowing rotor speed, electromagnetic torque, and stator current to return to normal levels once the fault is cleared. However, under extreme under-voltage conditions, such as a 60% voltage reduction, the motor's adaptive capacity is exceeded. This results in elevated thermal stress and an inability to restore normal operation post-fault, highlighting the need for protective measures at higher fault levels. The application of Ohm's law in this analysis confirmed that voltage reductions accompanied by compensatory current increases led to temporary decreases in effective resistance, facilitating adaptation under moderate conditions.

While this study focuses on under-voltage faults, the inclusion of other electrical (e.g., over-voltage, phase imbalance) and mechanical faults (e.g., rotor misalignment, load disturbances) in future work would offer a broader perspective. The reliability of the data was confirmed by comparing simulation results with theoretical benchmarks and performing sensitivity analyses to ensure robustness under varying motor parameters.

These findings emphasize the importance of defining appropriate protective thresholds and incorporating fault-tolerant designs in motor-driven systems. By establishing critical adaptive limits, the study contributes to the improvement of fault management practices, enabling enhanced motor reliability and operational continuity in power networks susceptible to voltage disturbances.

DISCLAIMER (ARTIFICIAL INTELLIGENCE)

Author(s) hereby declare that NO generative AI technologies such as Large Language Models (ChatGPT, COPILOT, etc) and text-to-image generators have been used during writing or editing of this manuscript.

COMPETING INTERESTS

Authors have declared that no competing interests exist.

REFERENCES

Abhinandan, A. C., & Sidram, M. H. (2017). Fault diagnosis of an induction motor through motor current signature analysis, FFT & DWT analysis. In 2017 4th IEEE International Conference on Engineering Technologies and Applied Sciences (ICETAS).

Bassey, J. B., Ekpo, D. D., & Gentle, V. U. (2024). Computational fluid dynamics analysis of flow characteristics in convergent and divergent sections. International Journal of Science, Engineering and Technology, 12(2).

Batool, M., & Ahmad, A. (2013). Mathematical modeling and speed torque analysis of three phase squirrel cage induction motor using Matlab Simulink for electrical machines laboratory. International Electrical Engineering Journal (IEEJ), 4(1), 880-889.

Cruz, S. M., & Cardoso, A. M. (2001). Stator winding fault diagnosis in three-phase synchronous and asynchronous motors, by the extended Park's vector approach. IEEE Transactions on Industry Applications, 37(5), 1227-1233.

de Almeida, A. T., Greenberg, S. F., & Rao, P. (2016). Electric motor systems efficiency. In Energy management and conservation handbook (pp. 343-370). CRC Press.

Diji, C. J., Ekpo, D. D., & Adadu, C. A. (2013). Design of a biomass power plant for a major commercial cluster in Ibadan-Nigeria. The International Journal of Engineering and Science, 2(3), 23-29.

Diji, C. J., Ekpo, D. D., & Adadu, C. A. (2013). Exegoenvironmental evaluation of a cement manufacturing process in Nigeria. International Journal of Engineering Research and Development, 7, 25-32.

Ejiofor, S. O., Abuchi, N. C., Damian, N., & Okoro, O. I. (2019). Performance study of three-phase induction motor driving a load. Discovery Journals, 55(282), 279-290.

Ekpo, D. D. (2012). Challenges of municipal solid waste disposal: A case study of Uyo township. Education & Science Journal of Policy Review & Curriculum Development, 1(2), 110-116.

Etim, P., Ekpo, D. D., Ekop, I. E., Bassey, J. E., Ononokpono, O. J., & Udobong, O. G. (2024). Design, fabrication and preliminary testing of a small-scale cassava starch extraction machine. Turkish Journal of Agriculture-Food Science and Technology, 12(8), 1448-1456.

Ezeonye, C. S., Nkan, I. E., Okpo, E. E., & Okoro, O. I. (2022). Dynamic analysis and computer simulation of interior permanent magnet synchronous motor with intermittent loading. Nigerian Journal of Technology, 41(1), 148-157.

Gonzalez, A., & Arjona, M. A. (2014). New starting system for three-phase induction motors by using a part-winding and capacitors. In 7th IET International Conference on Power Electronics, Machines and Drives (PEMD 2014), Manchester, England.

Jha, B., Panda, M. K., Pandey, P. K., & Pant, L. (2016). PSO-based online vector controlled induction motor drives. In 2016 International Conference on Electrical, Electronics, and Optimization Techniques (ICEEOT).

Lee, C. Y. (1999). Effects of unbalanced voltage on the operation performance of a three-

phase induction motor. IEEE Transactions on Energy Conversion, 14(2), 202-208.

Li, B., Chow, M. Y., Tipsuwan, Y., & Hung, J. C. (2000). Neural-network-based motor rolling bearing fault diagnosis. IEEE Transactions on Industrial Electronics, 47(5), 1060-1069.

Nandi, S., Toliyat, H. A., & Li, X. (2005). Condition monitoring and fault diagnosis of electrical motors—A review. IEEE Transactions on Energy Conversion, 20(4), 719-729.

Nkan, I. E., & Okpo, E. E. (2016). Electric power forecasting by the year 2020 using the least square method. International Journal of Research and Advancement in Engineering Science, 6(1), 205-215.

Nkan, I., Obi, P., Natala, H., & Okoro, O. (2023). Investigation of the transfer capability of the Nigerian 330 kV, 58-bus power system network using FACTS devices. ELEKTRIKA-Journal of Electrical Engineering, 22(1), 53-62.

Okpo, E. E., Le Roux, P. F., & Nnachi, A. F. (2023). Induction motor fault identification using support vector machine. In 2023 6th International Conference on Renewable Energy and Power Engineering (REPE).

Okpo, E. E., Okoro, O. I., Awah, C. C., & Akuru, U. B. (2019). Performance evaluation of 5.5 kW six-phase asynchronous motor. In 2019 IEEE PES/IAS PowerAfrica.

Okpo, E. E., Okoro, O. I., Awah, C. C., & Akuru, U. B. (2020). Investigating the dynamic behaviour of a six-phase induction motor under unbalanced faults. In 2020 IEEE PES/IAS PowerAfrica.

Siddique, A., Yadava, G., & Singh, B. (2004). Effects of voltage unbalance on induction motors. In Conference Record of the 2004 IEEE International Symposium on Electrical Insulation.

Sunday, A. B., Okpo, E. E., & Ekpo, D. D. (2024). Load rejection effects analysis on synchronous generators with ANN. American Journal of Engineering Research (AJER), 13(7), 57-65.

Udoh, D. E., Ekpo, D. D., & Nkan, I. E. (2024). Design and development of a package delivery robot. International Journal of Multidisciplinary Research and Analysis, 7(6), 2520-2526.

Williams, E. A., Okpo, E. E., & Nkan, I. E. (2023). Performance evaluation of induction motor behaviour on conventional and PV system power sources. International Journal of Multidisciplinary Research and Analysis, 6(12), 5500-5511.

Xiao, Y., Zhou, L., Wang, J., & Liu, J. (2018). Design and performance analysis of magnetic slot wedge application in double-fed asynchronous motor-generator by finite-element method. IET Electric Power Applications, 12(7), 1040-1047.

Disclaimer/Publisher's Note: The statements, opinions and data contained in all publications are solely those of the individual author(s) and contributor(s) and not of the publisher and/or the editor(s). This publisher and/or the editor(s) disclaim responsibility for any injury to people or property resulting from any ideas, methods, instructions or products referred to in the content.

© Copyright (2024): Author(s). The licensee is the journal publisher. This is an Open Access article distributed under the terms of the Creative Commons Attribution License (http://creativecommons.org/licenses/by/4.0), which permits unrestricted use, distribution, and reproduction in any medium, provided the original work is properly cited.

Peer-review history:
The peer review history for this paper can be accessed here:
https://www.sdiarticle5.com/review-history/128161